Identifying EphA2-Targeted Lead Compound in Breast Cancer

Mohd Nehal[1], Jahanarah Khatoon[1]

[1]Department of Biosciences, Integral University, Lucknow, 226026, Uttar Pradesh, India

Salman Akhtar[2], Mohammad Kalim Ahmad Khan[2*]

[2]Department of Bioengineering, Integral University, Lucknow, 226026, Uttar Pradesh, India

***Corresponding author**
Email: mkakhan@iul.ac.in

ABSTRACT

Ephrin Type-A receptor 2 (EphA2) plays a crucial role in breast cancer cell survival and proliferation, making it a promising therapeutic target. EphA2 overexpression is associated with poor prognosis and metastatic behavior in melanoma, lung, prostate, brain, breast cancer, and leukemia. In silico analysis identified Mcule-8617639093 as a potent EphA2 inhibitor. Through proliferation assays targeting EphA2 in MDA-MB-231 breast cancer cells, we found that the virtually identified lead molecule significantly bound to EphA2-overexpressing breast cancer cells at different concentrations. The efficacy of the compound was validated using MTT assays and annexin-V/PI staining. These findings contribute to the development of EphA2-targeted therapies

Keywords: EphA2, MDA-MB-231, Breast cancer, Lead compound, Mcule-8617639093

1. INTRODUCTION

Breast cancer is the second most common cancer globally and the second leading cause of cancer-related mortality among women worldwide after lung cancer [1]. It is the most prevalent malignancy among women, with a prevalence of 21.4% to 32% [2, 3]. Although breast cancer mainly affects older women, it can also occur in younger women [4]. The EPH-receptor is a member of the receptor tyrosine kinase family, which plays a critical role in tissue organization and development. Eph receptors were categorized into the Eph A and Eph B groups. The EphA family includes EphA1-EphA8 and EphA10, while the EphB family comprises EphB1-4 and EphB6. EphA1 was first identified during RTK receptor screening in 1987, and was discovered in the liver [5, 6]. The Eph receptor contains both extracellular and intracellular domains. The extracellular domain contains an active site for ligand binding, interacting with ephrin ligands to activate ephrin-EphA2-directed responses, such as differentiation, migration, and cell proliferation. Upon ligand binding, Eph increases its kinase activity, resulting in autophosphorylation [7]. Owing to membrane attachment, the Eph receptor enables forward and backward signaling. Overexpression of both Eph occurs in liver, melanoma, lung, colon, prostate, gastric, and breast cancers [6, 8]. The EphA2 receptor is an RTK receptor integrin protein on chromosome 1p36 that is restricted to proliferating epithelial cells in adults [9]. EphA2 predominantly binds to Ephrin A1 and functions as an anti-oncogenic or pro-oncogenic molecule. In the ligand-bound form, EphA2 acts as an anti-oncogenic agent, inhibiting cancer cell migration, tumor growth, and angiogenesis, whereas in the ligand-unbound form, it acts as a pro-oncogenic agent, leading to overexpression. EphA2 overexpression correlates with poor prognosis and metastasis in brain, prostate, lung, and breast cancers [10-13]. EphA2 promotes tumor cell invasion in colorectal carcinoma [14]. EphA2 can be targeted in antibody therapies that inhibit breast cancer xenografts and metastasis [15]. Preclinical research on antibody therapy has shown significant potential. In breast cancer, EphA2 is extensively expressed, enhancing malignant behavior and making it an effective therapeutic target. EphA2 mediates cell-cell interactions, adhesion, and migration. Inhibition of its expression may prevent or treat breast cancer.

In our previous research, compound Mcule-8617639093 was identified through in silico analysis using structure-based virtual

screening, molecular docking, and molecular dynamic simulation techniques [16-19, 20]. This approach identified the optimal molecule for targeting the target protein. In silico analysis, the most suitable molecule for protein binding through molecular docking and dynamic simulation methodologies [20]. The outcomes were validated through experimental procedures, which showed that the molecule exhibited the desired effect and effectively targeted the protein. This study was based on wet lab research, focusing on EphA2 in the MDA-MB-231 breast cancer cell line. Predicted lead molecule was validated using MTT assay, phase contrast microscopy, ROS, and Annexin-V/PI staining flow cytometry. These assays enabled the assessment of EphA2 expression levels and cell viability. MTT assays, phase contrast microscopy, ROS, and annexin-V/PI staining were used to evaluate the impact of EphA2 expression on cell viability.

2. METHODOLOGY

2.1. Chemicals and reagents

The inhibitor Mcule-8617639093 was procured from Mcule, Inc. (Palo Alto, CA, USA). Phosphate-buffered saline (PBS), antibiotic-antimycotic solution, trypsin, and MTT dye (Thiazolyl Blue Tetrazolium Bromide) were used. Fetal bovine serum (FBS) was obtained from Gibco (MA). DMEM media and 0.2-micron syringe filters were obtained from Sartorius AG (Göttingen, Germany), while DMSO and isopropanol were acquired from Sigma-Aldrich. The remaining materials were either drawn from existing laboratory stock or purchased from local suppliers. All chemicals used were of analytical grade. Standard procedures were adhered to during the execution of all experiments.

2.2. Cell lines and culture

MDA-MB-231 breast cancer cells were obtained from the National Center for Cell Science (NCCS), Pune, India. MDA-MB-231 cells were cultured in Dulbecco's modified Eagle's medium (DMEM) supplemented with 10% fetal bovine serum (FBS) and a 1% antibiotic–antimycotic solution. The cells were maintained in a 5% CO2 incubator at 37°C (New Brunswick Galaxy 170R; Eppendorf India Private Ltd., India).

2.3. Cytotoxicity assay

The MTT assay was used to evaluate the cytotoxic effects of Mcule-8617639093 on the MDA-MB-231 cell line. The cells (5x10^3 cells per well) were cultured in 96-well plates for 24 h at 37°C with 5% CO2 using DMEM (Dulbecco's Modified Eagle Media-AT149-IL) supplemented with 10%

FBS, FBSHIMEDIA-RM 10432, and 1% antibiotic solution [21]. The following day, the cells were exposed to varying concentrations of Mcule-8617639093 (5, 10, 20, 30, and 40 µM) and dasatinib (125–2000 nm). Incubation was continued for 24 h and 48 h under standard conditions, while the blank control cells remained untreated. After 24 and 48 h of culture, 10 µL of 5 mg/ml MTT solution was added and the culture was maintained for an additional 4 h. Upon completion of the experiment, the culture supernatant was removed, and the cell layer matrix was dissolved in 100 µL of dimethyl sulfoxide (DMSO). Absorbance was measured at 570 and 630 nm using a spectrophotometer (Bio-Rad, California, USA), and each cell was photographed with an AmScope digital camera (10 MP Aptima CMOS) under an inverted microscope (Olympus ek2). Untreated cells served as controls in all three experimental sets. The 50% inhibitory concentration (IC50) was determined using the GraphPad Prism 8.4. The results were expressed as a percentage of cell viability, calculated using the following formula: Cell viability (%) = (Average of At/Average of Ac) × 100, where At and Ac represent the absorbance of the treated and untreated control wells, respectively.

2.4. Examination of morphological alternation by phase contrast microcopy

MDA-MB-231 cells (5 × 103 cells per well) were co-cultured for 24 h with dasatinib (250 nM) and Mcule-8617639093 at concentrations of 5, 10, 20, 30, and 40 µM. Subsequently, images capturing the cellular morphological changes in both treated and untreated control cells were obtained using the relief phase channel of the FLoid imaging station (Thermo Scientific, United States).

2.5. DAPI/PI staining

Nuclear alterations in MDA-MB-231 cells were assessed using DAPI dye for cellular labeling. The cells, at a density of 1 × 104 per well, underwent a 24-hour treatment with mcule-8617639093 at concentrations ranging from 5 to 40 µM and dasatinib at 250 nM treatment, cells were washed with PBS and fixed in 4% paraformaldehyde for 10 min. Following fixation, the cells were permeabilized using buffer containing 0.25% Triton X-100 and stained with 300 nM DAPI. The cells were examined using a FLoid imaging station (Thermo Scientific, United States) with a blue filter.

2.6. Measurement of ROS in the cytosol

Reactive oxygen species (ROS) are generated through numerous processes, play a crucial role in cell cycling, act as signaling molecules during normal cell transduction, and exert

various biological effects at elevated concentrations. To detect cytosolic ROS in MDA-MB-231 cells, a fluorogenic dye (H2DCFDA) was used to detect. MDA-MB-231 cells (5 × 10^4 per well) were exposed to different concentrations of dasatinib (250 nM) and Mcule-8617639093 (ranging from 5 µM to 40 µM) for 6 h. Subsequently, cells were stained with 25 µM H2DCFDA for 30 min at 37°C. Excess dye was removed using phosphate-buffered saline (PBS). Following the removal of excess DCFH-DA, images were captured using a fluorescence microscope (Nikon ECLIPSE Ti-S, Japan). Finally, photomicrographs were obtained with a FLoid imaging station (Thermo Scientific, United States) utilizing its green fluorescence channel [22].

2.7. Apoptosis assay

Apoptotic cells were identified using annexin V/PI labeling. Phosphatidylserine was detected using Annexin-V, whereas necrotic cells were identified using propidium iodide (PI). As noted by Khan et al., 2020 [23], Annexin-V binds to phosphatidylserine, which becomes exposed on the outer leaflet of the plasma membrane during apoptosis, and PI serves as a membrane dye that marks cells with compromised membranes. Cells were cultivated in a 6-well plate at a density of 1X10^6 and exposed to varying concentrations of Mcule-8617639093 (5, 10, 20, 30, and 40 µM) and dasatinib (0.125–2 µM) for 24 h. The cells were harvested using sterile phosphate-buffered saline (PBS) at ice-cold temperatures. Subsequently, the cells were rinsed with PBS and subjected to three rounds of centrifugation in a ROTEK Laboratory centrifuge. An ice-cold 1X binding buffer was added to the pellet, followed by the addition of 5 µM propidium iodide (PI) and 5 µM Annexin V-FITC. The cells were incubated on ice in the dark for 15 min. Subsequently, 400 µM 1X binding buffer was added to the tube. The stained cells were immediately analyzed using FACSCalibur flow cytometry (BD Biosciences, San Diego, CA, USA).

3. RESULTS

Our previous research indicated that Mcule-8617639093 inhibits the overexpression of EphA2 in silico. However, the direct effect of Mcule-8617639093 on breast cancer cells remains unclear. Therefore, we initially evaluated the effects of Mcule-8617639093 on cell survival, viability, morphology, and apoptosis. These investigations enabled us to ascertain the therapeutic efficacy of Mcule-8617639093 and to elucidate its potential mechanism of action. The chemical structure of lead molecule is shown in Fig. 1.

Fig. 1. Chemical structure of Mcule-8617639093.

3.1. MTT assay

The cytotoxic effects of dasatinib and Mcule-8617639093 on MDA-MB-231 cells were assessed using an MTT assay. As depicted in Figure 4.3, cell viability exhibited an inverse relationship with both the concentration and exposure duration of Mcule-3034040298, thereby enhancing our understanding of the impact of small molecules on the mortality of MDA-MB-231 cell lines. An increase in the concentration of Mcule-8617639093 corresponded to a reduction in the number of colonies. MDA-MB-231 cells were cultured in 96-well plates with untreated cells serving as the control group. To evaluate cell proliferation, Mcule-8617639093 was administered at various concentrations (5, 10, 20, 30, and 40 µM) and dasatinib (250-2000 nM) for 24 and 48 h. Furthermore, Mcule-8617639093 reduced cell viability in a dose-dependent manner (Fig. 2). This indicates that the growth and viability of MDA-MB-231 cells were sensitive to both concentration and exposure time. The cell viability in Mcule-8617639093-treated cells was observed to be 83.65±5.79%, 73.79±5.54%, 53.71±5.05%, 32.70±5.81%, and 17.71±3.63% for 24 hours, and 74.97±4.07%, 2.51±6.12%, 37.92±6.06%, 12.76±2.90%, and 9.37±2.18% for 48 hours. Similarly, following treatment with dasatinib at various concentrations (125 nM, 250 nM, 500 nM, 1000 nM, and 2000 nM), cell viability was found to be 65.89±3.68%, 42.94±6.80%, 27.13±3.30%, 9.23±2.20%, and 3.17±1.29% for 24 hours, and 52.04±3.10%, 35.55±6.02%, 17.51±2.52%, and 3.52±1.31% for 48 hours, respectively. The IC50 values were determined to be 14.39 µM and 9.41 µM at 24 and 48 hours for Mcule-8617639093, and 196.5 nM and 142.5 nM at 24 and 48 hours for dasatinib, respectively. These findings suggest that Mcule-8617639093 may induce cytotoxicity and exhibit an antiproliferative effect on MDA-MB-231 cells.

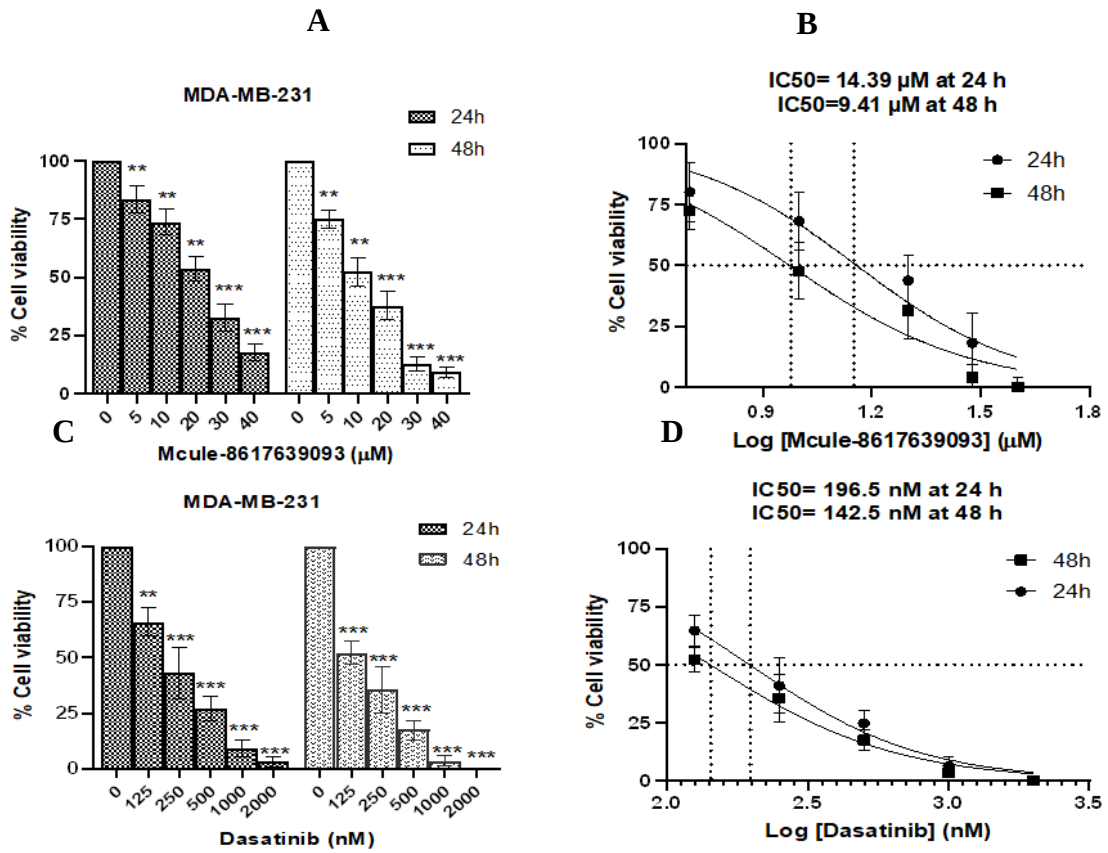

Fig. 2. Viability of MDA-MB-231 cells as a percentage, (A) Viability of cells treated with different concentrations of Mcul8617639093 (5-40 µM). (B) IC50 value of Mcule-8617639093 against MBA-MB-231 breast cancer cells. (C) Cell viability after being exposed to different dasatinib concentrations (125–2000 nM). (D) IC50 value of dasatinib against MBA-MB-231 breast cancer cells. The data displayed are the mean ± SEM of three separate experiments that were run in triplicate. (where *p<0.05, **p<0.01 and ***p<0.001 represent significant difference compared with control).

3.2. Examination of morphological alternation

Mcule-8617639093 at concentrations of 5, 10, 20, 30, and 40 µM, along with dasatinib at 250 nM, was administered to MDA-MB-231 cells to investigate morphological changes in breast cancer cells. All treated groups exhibited significant alterations in MDA-MB-231 cell morphology following a 24-hour exposure to Mcule-8617639093 and dasatinib. In contrast, the untreated control group displayed a well-spread, flattened cellular morphology, whereas all the treatment groups demonstrated a rounded morphology with cell shrinkage. A proportion of cells in each treatment group also exhibited membrane blebbing and lysis, indicating cytotoxic effects at the specified dosages (Fig. 3). As the treatment

concentration increased from 5 to 40 µM, the morphological changes in MDA-MB-231 cells progressively intensified across all treated groups.

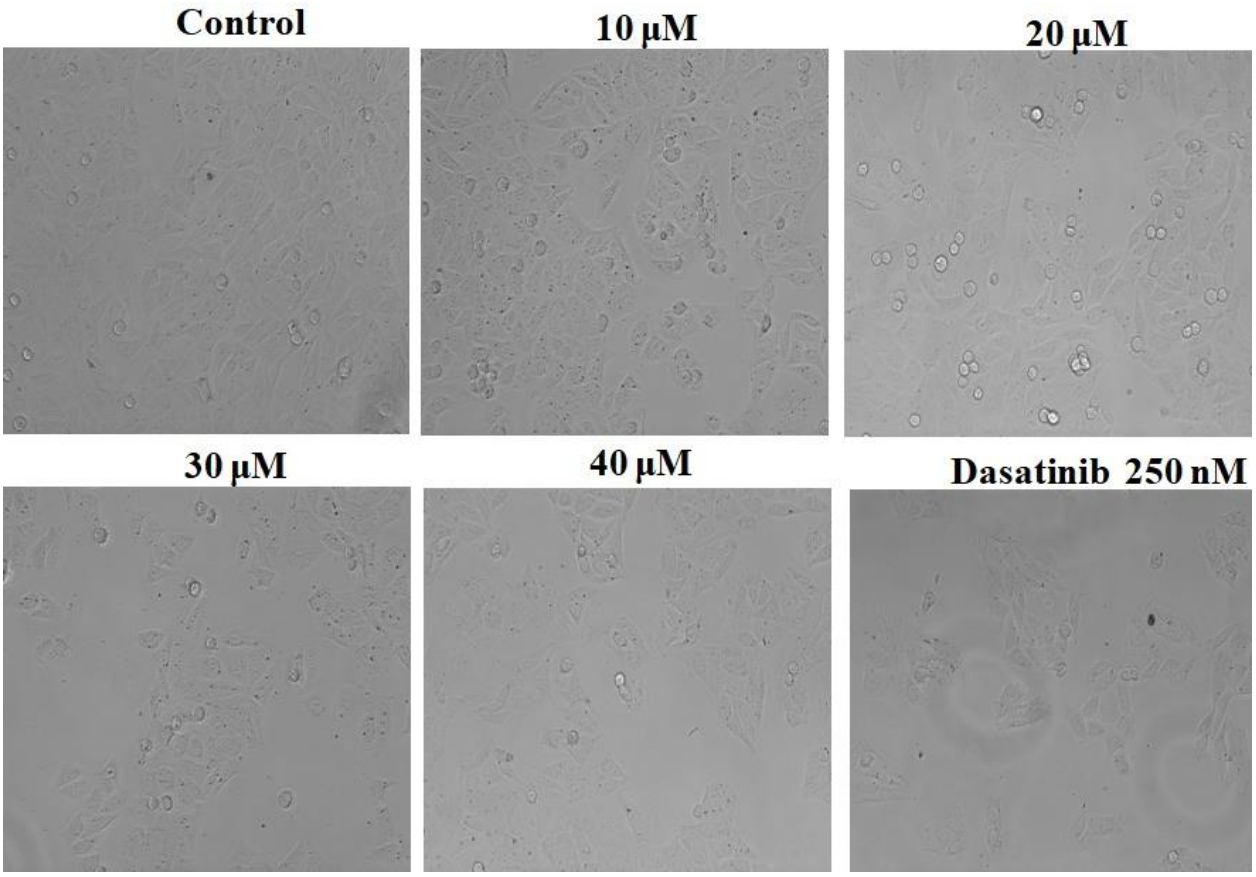

Fig.3. Phase contrast microscopy was used to study the cytomorphological pictures of MDA-MB-231 cells treated with dasatinib (250 nM) with Mcule-8617639093 at varying concentrations (10–40 µM) for 24 hours. The images displayed (magnification ×20; scale bar 100 µm) are representative of three separate studies carried out in triplicate.

3.3. Mcule-8617639093-induced nuclear condensation

DAPI staining was used to investigate apoptotic nuclear alterations following treatment with dasatinib and Mcule-8617639093, as illustrated in Fig. 4. Analysis of the images revealed that untreated cells exhibited uniform stain distribution and enhanced fluorescence with intact nuclear material. In contrast, cells treated with dasatinib and Mcule-8617639093 showed reduced fluorescence, accompanied by apoptotic bodies, nuclear membrane disintegration, and cellular membrane blebbing. Treatment with dasatinib and Mcule-8617639093 induced cell death. The images depict morphological changes in the cells post-treatment, including nuclear protrusions, condensation, disintegration, and the presence of apoptotic bodies. These

visual indicators strongly suggest programmed cell death and are commonly recognized as markers of apoptosis.

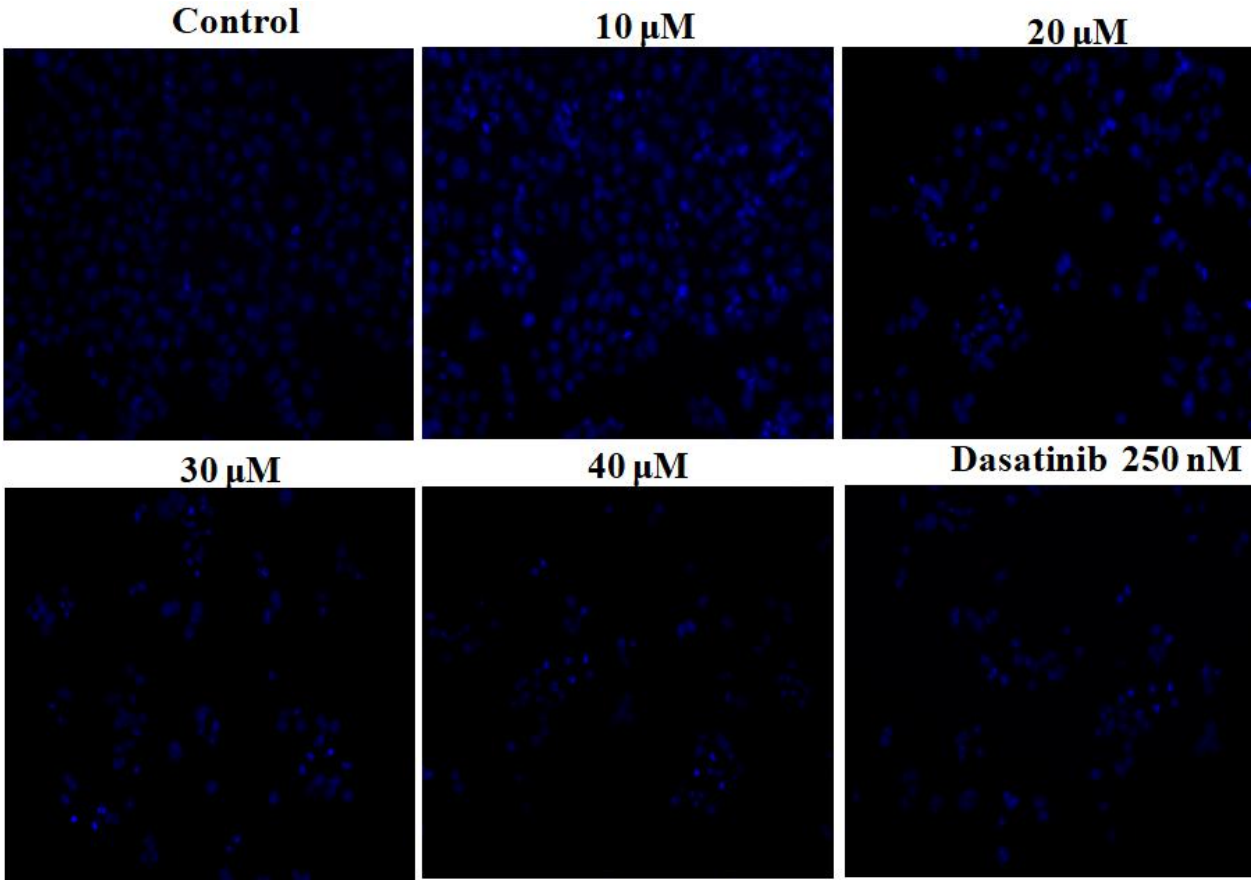

Fig.4. Nuclear condensation analysis in breast cancer MDA-MB-231 cells treated with dasatinib (250 nM) and Mcule-8617639093 at varying concentrations (10–40 µM) for 24 hours. The pictures displayed are typical of three independent experiments performed in triplicate (magnification ×20; scale bar 100 µm).

3.4. Measurement of intracellular ROS level

It is widely acknowledged that cancerous cells, when subjected to stressors, such as pharmacological treatment or radiation therapy, generate reactive oxygen species (ROS) as a consequence of oxidative stress. ROS production is considered a fundamental signal that initiates apoptosis. DCFH-DA was used to assess ROS production in MDA-MB-231 cells following the administration of dasatinib and Mcule-8617639093. Treatment with increasing concentrations of Mcule-8617639093 (10–40 µM) resulted in a corresponding increase in ROS levels, as illustrated in the photomicrographs (Fig. 5).

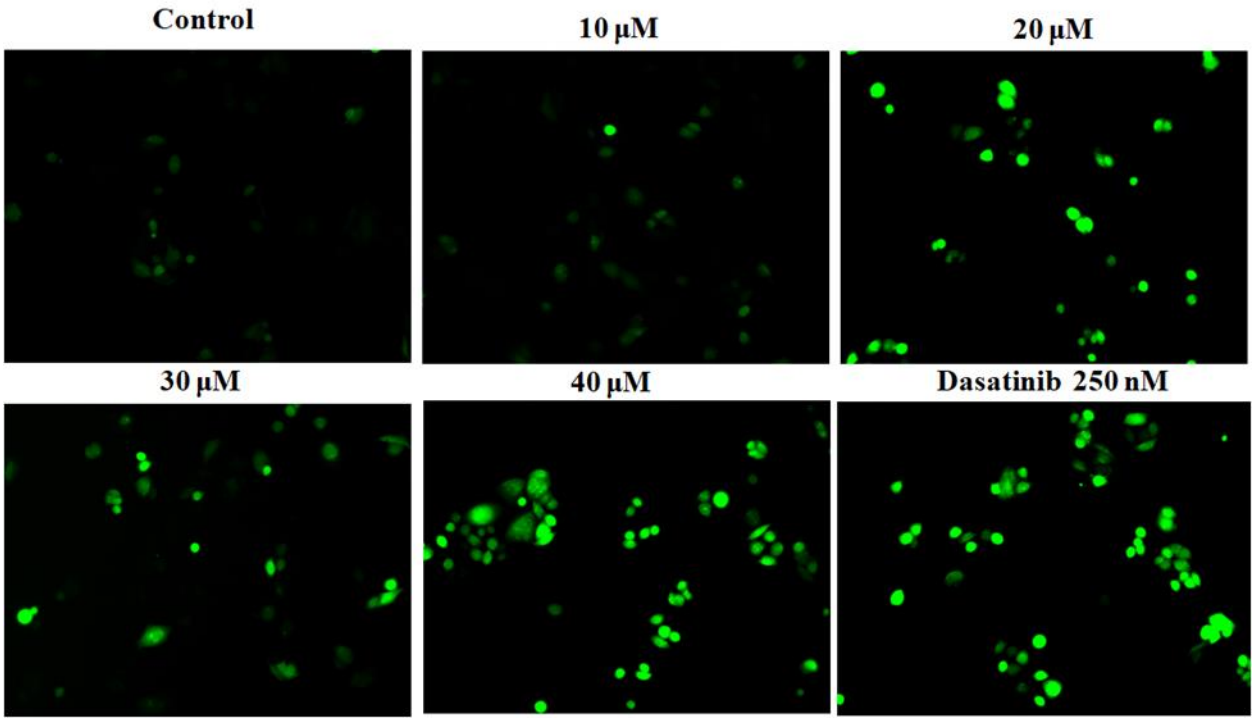

Fig.5. Fluorescent photomicrographs of MDA-MB-231 cells after 12 hours using DCFH-DA stained Mcule-8617639093 at various concentrations (10–40 µM) and dasatinib (250 nm) reveal elevated ROS.

3.5. Annexin-V/ PI staining assay

To examine the role of Mcule-8617639093 and dasatinib in inducing apoptosis, MDA-MB-231 cells were treated with 5, 10, 20, 30, and 40 µM Mcule-8617639093 and 0.125, 0.250, 0.50, 1, and 2 µM for dasatinib. The control group consisted of untreated cells. In this study, we aimed to quantify the dose-dependent effects of these treatments on apoptosis. The annexin-V/PI staining method was used to identify cells undergoing apoptosis or programmed cell death. The experimental results, as depicted in Figure 6, demonstrated an increase in apoptosis with varying concentrations of dasatinib and Mcule-8617639093 compared to the control. In untreated cells, the percentage of dead cells was 0.17%, whereas the viable fraction was 95.16%. Conversely, early and late apoptosis were observed at 4.34% and 0.33%, respectively. These findings indicated a significant increase in apoptosis following compound incubation, resulting in a reduction in the percentage of viable cells. After a 24-hour treatment with 10, 20, 30, and 40 µM Mcule-8617639093, cell viability was 71.16 %, 29.29 %, 27.22 %, and 20.24 %, respectively. Additionally, after 24 h of

dasatinib treatment, cell viability was 39.98%, 3.33%, 4.39%, and 5.56% at concentrations of 0.125, 0.250, 0.50, 1, and 2 µM, respectively. However, as shown in Fig.6. the blank control did not significantly induce cell death. Therefore, Mcule-8617639093 induces dose-dependent apoptosis in breast cancer cells.

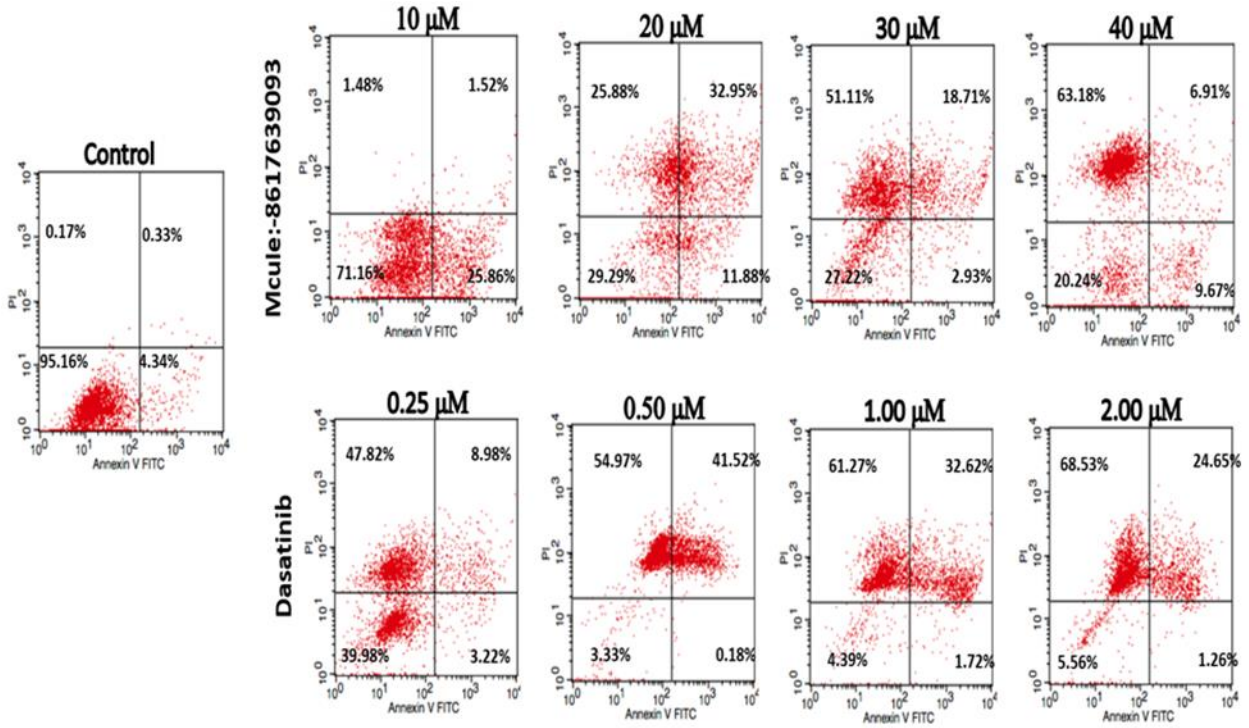

Fig.6. Flow cytometry images demonstrate the apoptotic effects of dasatinib and Mcule-8617639093, utilizing Annexin V-FITC/PI staining. The breast cancer MDA-MB-231 cells were treated with Mcule-8617639093 (10–40 µM) and dasatinib (0.25–2 µM) at varying concentrations for 24 hours, as determined by flow cytometry analysis. The histogram's upper left (UL) quadrant shows apoptotic cells, while the upper right (UR) and lower left (LL) quadrants show late apoptosis, viable cells, and early apoptotic cells, respectively. Three separate experiments are represented by the data displayed.

4. DISCUSSION

Breast cancer continues to be the predominant cause of cancer-related mortality among women globally, with triple-negative breast cancer (TNBC) being notably aggressive and resistant to standard therapies. The limited efficacy of current treatment modalities, primarily owing to drug resistance and tumor recurrence, highlights the urgent need for novel therapeutic agents with improved efficacy and reduced adverse effects. In this context, the present study assessed the anti-cancer potential of Mcule-8617639093, a small molecule previously identified through in silico screening, as a potential EphA2 inhibitor, in comparison with the established tyrosine kinase inhibitor

dasatinib, against the TNBC cell line MDA-MB-231. To evaluate the cytotoxic potential of Mcule-8617639093, an MTT assay was conducted 24 and 48 h post-treatment. The results demonstrated a dose- and time-dependent reduction in cell viability after treatment with Mcule-8617639093. Specifically, cell viability significantly decreased with increasing concentrations, indicating a strong antiproliferative effect. The IC_{50} values of Mcule-8617639093 were calculated to be 14.39 µM and 9.41 µM at 24 and 48 hours, respectively, highlighting its enhanced efficacy over time. Comparatively, dasatinib displayed a lower IC_{50} (196.5 nM and 142.5 nM), yet Mcule-8617639093 demonstrated a clear cytotoxic profile indicative of its potential therapeutic promise. Microscopic evaluation of the treated cells revealed distinct morphological alterations, including cell shrinkage, membrane blebbing, and rounding, which intensified in a concentration-dependent manner. These morphological changes are characteristic hallmarks of apoptotic cell death and suggest that the cytotoxic mechanism of the compound may involve the induction of apoptosis. To confirm apoptosis, DAPI staining was conducted to examine the nuclear morphology. The treated cells showed condensed, fragmented nuclei with visible apoptotic bodies, further supporting the hypothesis of Mcule-8617639093-mediated apoptosis. In contrast, the untreated control cells retained intact and evenly stained nuclei. These observations are consistent with apoptosis-related nuclear disintegration and chromatin condensation. Furthermore, ROS generation, an early event in apoptotic signaling, was evaluated using DCFH-DA staining. An increase in intracellular ROS levels was observed in the Mcule-8617639093-treated cells in a dose-dependent manner. This increase in ROS may act as a key upstream signal that initiates apoptotic cascades, supporting the role of oxidative stress in the mechanism of action of the compound. Finally, annexin V/PI dual staining coupled with flow cytometry was used to quantify apoptotic cell populations. The results revealed a marked increase in both early and late apoptotic cells upon treatment with Mcule-8617639093, particularly at higher concentrations. This confirmed that the observed decrease in cell viability was primarily due to apoptosis rather than necrosis or other forms of cell death. Compared with dasatinib, Mcule-8617639093 induced a significant apoptotic response, although at a higher concentration range. Collectively, these data strongly suggested that Mcule-8617639093 exerts

potent cytotoxic and pro-apoptotic effects on MDA-MB-231 breast cancer cells through mechanisms involving morphological disruption, nuclear condensation, oxidative stress via ROS generation, and apoptosis induction. These findings provide promising experimental evidence for the potential of this compound as a novel therapeutic candidate for triple-negative treatment. Further studies, including mechanistic pathway analysis, target validation, and in vivo efficacy studies, are warranted to establish its clinical relevance.

5. CONCLUSION

This study demonstrated that Mcule-8617639093 effectively inhibits the overexpression of EphA2, a receptor tyrosine kinase associated with poor prognosis in breast cancer. In MDA-MB-231 cells, Mcule-8617639093 exhibited potent antiproliferative and pro-apoptotic effects in a dose- and time-dependent manner, as evidenced by MTT assay, morphological alterations, ROS generation, nuclear condensation, and Annexin-V/PI-based apoptosis analysis. Its high specificity and strong cytotoxic activity suggest that Mcule-8617639093 is a promising candidate for further in vivo evaluation as a targeted therapeutic agent for triple-negative breast cancer.

ACKNOWLEDGEMENT

The authors express their sincere gratitude to the Central Instrumentation Facility at Integral University, Lucknow, for granting access to advanced equipment and essential resources that were crucial for the successful execution of this research.

REFERENCES

1. Sukocheva O. A. (2018). Expansion of Sphingosine Kinase and Sphingosine-1-Phosphate Receptor Function in Normal and Cancer Cells: From Membrane Restructuring to Mediation of Estrogen Signaling and Stem Cell Programming. International journal of molecular sciences, 19(2), 420. https://doi.org/10.3390/ijms19020420

2. Fuemmeler, B. F., Pendzich, M. K., & Tercyak, K. P. (2009). Weight, dietary behavior, and physical activity in childhood and adolescence: implications for adult cancer risk. Obesity facts, 2(3), 179–186. https://doi.org/10.1159/000220605
3. Harirchi, I., Karbakhsh, M., Kashefi, A., & Momtahen, A. J. (2004). Breast cancer in Iran: results of a multi-center study. Asian Pacific journal of cancer prevention : APJCP, 5(1), 24–27.
4. Campbell-Enns, H. J., & Woodgate, R. L. (2017). The psychosocial experiences of women with breast cancer across the lifespan: a systematic review. Psycho-oncology, 26(11), 1711–1721. https://doi.org/10.1002/pon.4281
5. Zhao, P., Jiang, D., Huang, Y., & Chen, C. (2021). EphA2: A promising therapeutic target in breast cancer. Journal of genetics and genomics = Yi chuan xue bao, 48(4), 261–267. https://doi.org/10.1016/j.jgg.2021.02.011.
6. Udayakumar, D., Zhang, G., Ji, Z., Njauw, C. N., Mroz, P., & Tsao, H. (2011). EphA2 is a critical oncogene in melanoma. Oncogene, 30(50), 4921–4929. https://doi.org/10.1038/onc.2011.210
7. Eisen, A., Bhatt, D. L., Steg, P. G., Eagle, K. A., Goto, S., Guo, J., Smith, S. C., Ohman, E. M., Scirica, B. M., & REACH Registry Investigators (2016). Angina and Future Cardiovascular Events in Stable Patients With Coronary Artery Disease: Insights From the Reduction of Atherothrombosis for Continued Health (REACH) Registry. Journal of the American Heart Association, 5(10), e004080. https://doi.org/10.1161/JAHA.116.004080
8. Tandon, M., Vemula, S. V., & Mittal, S. K. (2011). Emerging strategies for EphA2 receptor targeting for cancer therapeutics. Expert opinion on therapeutic targets, 15(1), 31–51. https://doi.org/10.1517/14728222.2011.538682
9. Lorico, A., & Rappa, G. (2011). Phenotypic heterogeneity of breast cancer stem cells. Journal of oncology, 2011, 135039. https://doi.org/10.1155/2011/135039
10. Kurose, H., Ueda, K., Kondo, R., Ogasawara, S., Kusano, H., Sanada, S., Naito, Y., Nakiri, M., Nishihara, K., Kakuma, T., Akiba, J., Igawa, T., & Yano, H. (2019). Elevated Expression of EPHA2 Is Associated With Poor Prognosis After Radical Prostatectomy in Prostate Cancer. Anticancer research, 39(11), 6249–6257. https://doi.org/10.21873/anticanres.13834
11. Alonso-C, L. M., Trinidad, E. M., de Garcillan, B., Ballesteros, M., Castellanos, M., Cotillo, I., Muñoz, J. J., & Zapata, A. G. (2009). Expression profile of Eph receptors and ephrin ligands in healthy human B lymphocytes and chronic lymphocytic leukemia B-cells. Leukemia research, 33(3), 395–406. https://doi.org/10.1016/j.leukres.2008.08.010
12. Trinidad, E. M., Zapata, A. G., & Alonso-Colmenar, L. M. (2010). Eph-ephrin bidirectional signaling comes into the context of lymphocyte transendothelial migration. Cell adhesion & migration, 4(3), 363–367. https://doi.org/10.4161/cam.4.3.11586
13. T Takahashi, Y., Itoh, M., Nara, N., & Tohda, S. (2014). Effect of EPH-ephrin signaling on the growth of human leukemia cells. Anticancer research, 34(6), 2913–2918.
14. Dunne, P. D., Dasgupta, S., Blayney, J. K., McArt, D. G., Redmond, K. L., Weir, J. A., Bradley, C. A., Sasazuki, T., Shirasawa, S., Wang, T., Srivastava, S., Ong, C. W., Arthur, K., Salto-Tellez, M., Wilson, R. H., Johnston, P. G., & Van Schaeybroeck, S. (2016). EphA2 Expression Is a Key Driver of Migration and Invasion and a Poor Prognostic Marker in Colorectal Cancer. Clinical cancer research : an official journal of the American Association for Cancer Research, 22(1), 230–242. https://doi.org/10.1158/1078-0432.CCR-15-0603

15. Z Zhang, T., Li, J., Ma, X., Yang, Y., Sun, W., Jin, W., Wang, L., He, Y., Yang, F., Yi, Z., Hua, Y., Liu, M., Chen, Y., & Cai, Z. (2018). Inhibition of HDACs-EphA2 Signaling Axis with WW437 Demonstrates Promising Preclinical Antitumor Activity in Breast Cancer. EBioMedicine, 31, 276–286. https://doi.org/10.1016/j.ebiom.2018.05.003
16. Khan, F. I., Lai, D., Anwer, R., Azim, I., & Khan, M. K. A. (2020). Identifying novel sphingosine kinase 1 inhibitors as therapeutics against breast cancer. Journal of enzyme inhibition and medicinal chemistry, 35(1), 172–186. https://doi.org/10.1080/14756366.2019.1692828
17. Khan, M. K. A., Akhtar, S., & Arif, J. M. (2018). Development of In Silico Protocols to Predict Structural Insights into the Metabolic Activation Pathways of Xenobiotics. Interdisciplinary sciences, computational life sciences, 10(2), 329–345. https://doi.org/10.1007/s12539-017-0237-4
18. Xiao, T., Xiao, Y., Wang, W., Tang, Y. Y., Xiao, Z., & Su, M. (2020). Targeting EphA2 in cancer. Journal of hematology & oncology, 13(1), 114. https://doi.org/10.1186/s13045-020-00944-9
19. Zhao, P., Jiang, D., Huang, Y., & Chen, C. (2021). EphA2: A promising therapeutic target in breast cancer. Journal of genetics and genomics = Yi chuan xue bao, 48(4), 261–267. https://doi.org/10.1016/j.jgg.2021.02.011
20. Mohd Nehal, Jahanarah Khatoon, Salman Akhtar, & Ahmad Khan, M. K. (2024). Computational insights into inhibiting EphA2: Integrating structure-based virtual screening, docking, and molecular dynamics simulations for small molecule discovery. Cellular and molecular biology (Noisy-le-Grand, France), 70(8), 16–31. https://doi.org/10.14715/cmb/2024.70.8.3
21. Buranaamnuay K. (2021). The MTT assay application to measure the viability of spermatozoa: A variety of the assay protocols. Open veterinary journal, 11(2), 251–269. https://doi.org/10.5455/OVJ.2021.v11.i2.9
22. Mishra, P., Ali Ahmad, M. F., Al-Keridis, L. A., Saeed, M., Alshammari, N., Alabdallah, N. M., Tiwari, R. K., Ahmad, A., Verma, M., Fatima, S., & Ansari, I. A. (2023). Methotrexate-conjugated zinc oxide nanoparticles exert a substantially improved cytotoxic effect on lung cancer cells by inducing apoptosis. Frontiers in pharmacology, 14, 1194578. https://doi.org/10.3389/fphar.2023.1194578
23. Khan, I., Mahfooz, S., & Ansari, I. A. (2020). Antiproliferative and Apoptotic Properties of Andrographolide Against Human Colon Cancer DLD1 Cell Line. Endocrine, metabolic & immune disorders drug targets, 20(6), 930–942. https://doi.org/10.2174/1871530319666191125111920